# Adsorption Characteristics of Perfluorosulfonic Acid Membrane Decomposition Products on a Platinum Electrode: An EQCM Study

**Jason M. Christ,[1] Charles B. Staub,[2] Ryan Richards,[1] and Huyen N. Dinh [3,*,z]**

[1]*Department of Chemistry and Geochemistry, Colorado School of Mines, Golden, Colorado 80401, USA*
[2]*Department of Chemical Engineering, University of South Carolina, Columbia, South Carolina 29208, USA*
[3]*Chemical Materials and Science Center, National Renewable Energy Laboratory, Golden, Colorado 80401, USA*

As hydrogen fuel cell vehicles move closer to mass commercialization, understanding the voltage losses due to contamination on low loading catalyst layers has become critical. It is imperative that contamination mechanisms are understood to mitigate these losses. In some cases, chemical breakdown of the polymer membrane can lead to formation of small molecules that can infiltrate and adsorb onto the catalyst layer, resulting in lower fuel cell performance and durability. Surface coverages of perfluorinated acid model compounds, representing polymer electrolyte membrane (PEM) chemical degradation products, were studied using an electrochemical quartz crystal microbalance (EQCM) with a polycrystalline platinum electrode. Perfluorosulfonic acid model compounds with a terminal sulfonic acid group exhibited no adsorption and no mass change. A similar model compound with a terminal carboxylic acid functional group exhibited higher surface coverage and stronger adsorption strength. Perfluorinated diacids, representing degradation products of a Nafion and 3M membrane, both showed mass increases well into the Pt oxide region, suggesting that the compounds were not fully displaced by surface oxides and that the terminal sulfonic acid group played a secondary role in the adsorption. Both perfluorinated chain length and functional group were found to play important roles in Pt surface adsorption characteristics.

 [DOI: 10.1149/2.0841813jes]

Manuscript submitted April 2, 2018; revised manuscript received September 26, 2018. Published October 6, 2018.

Polymer electrolyte membrane fuel cells (PEMFCs) are on the verge of becoming a significant source of energy production worldwide. Hydrogen fuel cell vehicles (FCV) are already commercialized in small volumes and on the road. FCVs must be as durable, reliable and cost-effective as current combustion engine vehicles. DOE's target for FCVs is 5,000 hours (equivalent to ca. 150,000 miles of driving) with less than 10% loss of performance.[1] A few millivolts loss due to contamination can have a big impact on the efficiency and operational lifetime of hydrogen fuel cell vehicles, especially for low loading catalyst FCVs. Performance durability losses originating in the membrane electrode assembly (MEA) continue to hinder progress. Although there are many known causes for durability loss, one such cause is due to system contamination. Numerous sources of contaminating compounds, i.e. chemical species adversely poisoning the membrane electrode assembly (MEA) while not participating in the electrochemical reactions to produce current, can be found in PEMFCs. Air at the cathode,[2–6] fuel at the anode,[7–12] balance of plant (BOP) components,[13–18] and MEA materials have all been shown to contain and/or produce contaminating species, either through impurities or chemical degradation of components. These species, in turn, can adsorb onto the electrocatalyst layer and/or infiltrate the MEA and affect performance.

Studies involving commercial membranes and model compounds have shown that when PFSA membranes are exposed to certain peroxides and hydroxyl radicals, various chemical decomposition compounds are produced.[19–21] Two compounds in particular, perfluoro (2-methyl-3-oxa-5-sulfonic pentanoic) acid (DA-Naf) and perfluoro (4-sulfonic butanoic) acid (DA-3M), both are shown in Figure 1, arise, along with HF, as the main membrane degradation compounds of Nafion and a 3M commercial PFSA membrane, respectively.[21,22] Although these membranes are similar in both performance and structure, variations in the perfluorinated carbon side chain, which are also seen in their chemical degradation products, (Figure 1) can lead to differences in catalyst poisoning. The aforementioned degradation products (DA-Naf and DA-3M) have been shown to adsorb on Pt-based electrocatalysts, leading to a loss in catalyst electrochemical surface area (ECSA), oxygen reduction reaction (ORR) activity, or both.[23] Along with model degradation compounds DA-Naf and DA-3M (diacids each containing a carboxylic acid and sulfonic acid moiety), model compound nonafluoro-1-butanesulfonic acid (SA1) (Figure 1) was chosen to gain fundamental insight on the adsorption effects solely due to the sulfonic acid i.e. sulfonate anion functional group. In addition, trifluoroacetic acid (TFA) (Figure 1), and undecafluorohexanoic acid (UFA) (Figure 1) were chosen to gain fundamental insight on the adsorption effects solely due to the carboxylic acid i.e. carboxylate anion functional group, as well as that of the fluorocarbon chain length.

Many successful attempts have been made to quantify the impact that certain contaminants inflict on performance, by measuring the in-situ current and voltage losses of operating fuel cells, and by determining the decreases in specific and mass activity of platinum-based electrodes via ex-situ studies.[3,11,12,23–27] While much useful information was gleaned from the results of previous fuel cell performance studies, adsorption mechanisms and surface coverages of certain contaminants e.g. PEM chemical degradation products DA-Naf and DA-3M, remain elusive.[28]

For example, 3M recently reported a voltage decay within the first 200 hours of a fuel cell accelerated stress test (AST) using their new perfluoro imide acid (PFIA) membrane, along with an increase in cell resistance near the end of life.[29] Analytical characterization of the PEMFC effluent water, collected during AST, showed a variety of small molecule fragments that could be traced to the membrane side chain. The authors inferred that the degradation process involved the PFIA ionomer side chain, but they do not know which side chain fragment or the mechanism that resulted in the fuel cell degradation observed during AST. It is of vital importance that a systematic study of the effect of membrane degradation products with different terminal functional groups and/or different chain lengths be carried out to gain a better understanding of the degradation mechanism.

Common cyclic voltammetry techniques used to measure ECSA e.g. integration of the hydrogen underpotential deposition (HUPD) region, are unable to accurately measure surface coverage of some anionic species due to the superimposition of anion and hydrogen atom adsorption and desorption currents.[30] Also, since most electrochemical methods used to measure ECSA are done at lower potentials (0.025–0.4 V), comparing losses in ORR activity (measured at higher

*Electrochemical Society Member.
zE-mail: Huyen.Dinh@nrel.gov

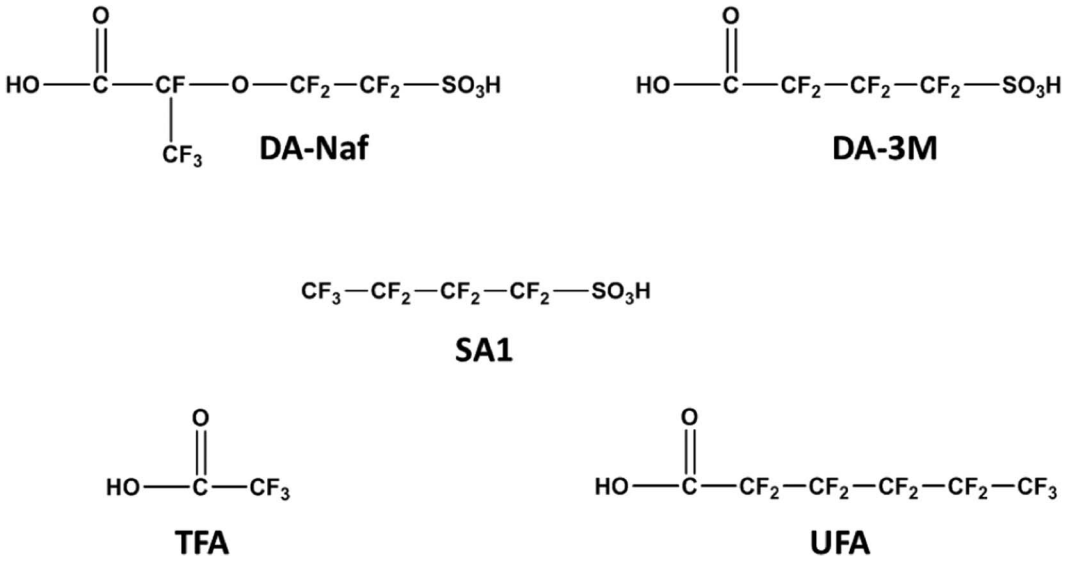


**Figure 1.** Chemical structures of the perfluorinated model compounds studied as contaminants.

potential: 0.9 V) is questionable. Simply determining if certain contaminants adsorb or not using cyclic voltammetry alone can also be challenging, as not all adsorption processes involve the charge transfer step necessary to invoke a change in measured current.[31]

Certain electrochemical techniques have been developed, e.g. electrochemical quartz crystal microbalance (EQCM) and surface-enhanced infrared absorption spectroscopy (SEIRAS),[32] to understand adsorption characteristics of chemical species occurring at an electrode surface under potential control. For this study, EQCM analysis was employed to determine surface coverages of perfluorinated organic acids, in the form of model compounds representing PEM chemical degradation products, at various concentrations and potentials using a polycrystalline Pt electrode.

## Experimental

Electrochemical measurements were taken using an Autolab PGSTAT302N equipped with an EQCM module. The EQCM module, fitted with a 6 MHz oscillator, was used to measure frequency changes of AT-cut quartz crystals with a resonant frequency of 6 MHz and vapor deposited Pt on a $TiO_2$ seed layer on either side (Metrohm). A $Pd/H_2$ electrode and a gold coil were used as the reference and counter electrode, respectively. All potentials are reported vs a reversible hydrogen electrode (RHE). Experiments were performed at room temperature in a polypropylene EQCM cell (Metrohm) purged with 99.9999% pure nitrogen (Matheson Tri Gas). All measurements were taken at a scan rate of 50 mV/s and performed in 0.1 M perchloric acid electrolyte (diluted from 70% $HClO_4$ double distilled veritas grade, GFS Chemical). DA-Naf and DA-3M were obtained in their lithium salt forms from collaborators at 3M with a reported purity of >95% and the major detected trace component being LiF. No adsorption effects of LiF at any concentration relevant to this study were observed in an internal investigation using a polycrystalline Pt electrode (data not shown). Consequently, it was determined that the LiF impurity would pose minimal interference with model compound adsorption. UFA was obtained from SynQuest Laboratories with a reported purity of 99%. SA1 and TFA were obtained from Sigma Aldrich with reported purities of 97% and 99% respectively. All compounds were used as received.

After electrochemical break-in of the Pt electrode (50 cycles, 0.025–1.2 V at 500 mV/s), baseline CV and EQCM frequency responses were recorded simultaneously. Electrochemical potential was held at 0.025 V while the frequency response was normalized to zero, and then scanned to 1.2 V and back for 3 cycles. A small aliquot of model compound solution (aqueous) was then injected into the cell to produce a specific concentration. Pt CV and EQCM signals, in the presence of model compounds, were subsequently measured following the same protocol and compared with baseline scans. All data shown are from the last of three overlapping potential cycles, which began immediately after the break-in procedure. For results involving multiple concentrations, all experiments were performed consecutively on the same electrode surface, while incrementally increasing the model compound concentration in the cell after CV and mass signals were recorded. ECSA of the Pt surface was measured through integration of the HUPD region from the baseline CV.

## Results and Discussion

Mass changes for all experiments were calculated according to the Sauerbrey equation,[33] described in Eq. 1:

$$\Delta m = -\frac{\Delta f \cdot \sqrt{\rho_q \mu_q}}{2n \cdot f_o^2} \quad [1]$$

Where $\Delta$m is the change in mass, $\Delta$f is the change in resonant frequency of the quartz crystal, $\rho_q$ is the density of quartz (2.648 g/cm$^3$), $\mu_q$ is the shear modulus of quartz ($2.947 \times 10^{11}$ g/(cm $\cdot$ s$^2$)), n is the number of harmonic at which the crystal is driven (set to 1 by design), and $f_o$ is the resonant frequency of the fundamental mode of the loaded crystal (6 MHz). It should be noted that the Sauerbrey equation as described above assumes an atomically flat and rigid electrode surface. This deviates slightly from the roughness factor of 1.6 found for the rigid polycrystalline Pt electrodes used in this study. Recently, a logarithmic dependence was found between Pt electrode surface roughness and frequency response during EQCM measurements, which in turn, can lead to under-evaluation of mass changes at the electrode interface if a correction to the experimental characteristic constant and/or modification to the Sauerbrey equation is not made.[34,35] It was determined that for an electrode roughness factor of 1.6, and given the low molecular weights of the model compounds involved in this study, the deviation here would account for less than 5% difference in mass change,[34] hence no corrections were made for this work. The small molecules reported here do not polymerize or bond together on the surface, and hence would not create a non-rigid crystalline structure. Furthermore, given the low concentration of the model compounds used (0.1 mM), it can be reasonably assumed that the rigid body requirement for the Sauerbrey equation was upheld, as reported by others.[36–38] Finally, given the low concentration of electrolyte used and short experimental times, surface roughness changes

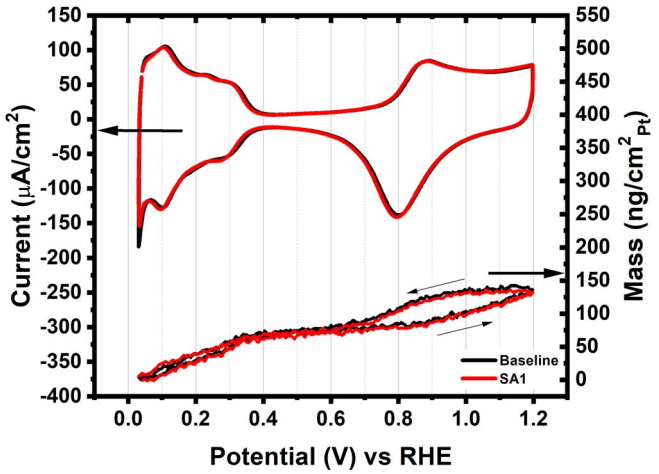


**Figure 2.** Voltammetric and EQCM response for SA1 adsorption on polycrystalline Pt. Black: 0.1M $HClO_4$ baseline CV and EQCM, red: SA1 (0.1 mM in 0.1M $HClO_4$) CV and EQCM. Thin arrows show direction of EQCM scan.

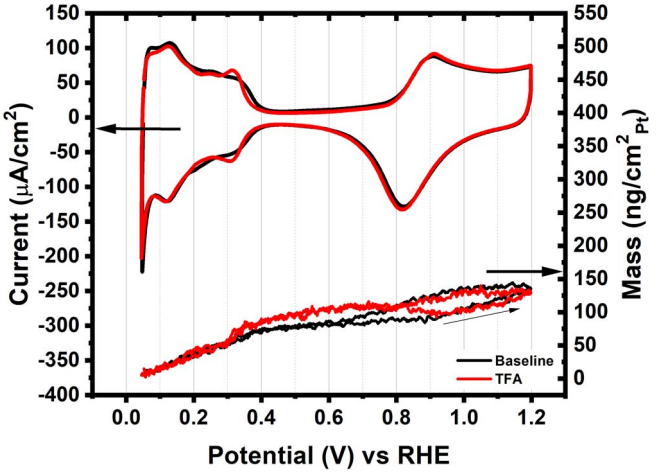


**Figure 3.** Voltammetric and EQCM response for TFA adsorption on polycrystalline Pt. Black: 0.1M $HClO_4$ baseline CV and EQCM, red: SA1 (0.1 mM in 0.1M $HClO_4$) CV and EQCM. Thin arrows show direction of EQCM scan.

due to Pt dissolution were considered to be negligible.[36] Surface coverages for all adsorbed species measured were calculated according to Eq. 2:

$$\theta = \frac{\Delta m \cdot MW^{-1}}{\frac{1}{2} C_{HUPD} \cdot F^{-1}} \quad [2]$$

Where θ is surface coverage (ratio of the moles of adsorbed model compound per moles of surface Pt), Δm is change in mass (calculated (Eq. 1) as the difference between baseline and model compound containing scans), MW is the molecular weight of injected model compound, $C_{HUPD}$ is the integrated charge of the HUPD region from the baseline scan, and *F* is the Faraday constant. The constant "1/2" is the assumption that every molecule adsorbed requires two Pt sites.[40,41]

CV and EQCM results under baseline conditions (polycrystalline Pt in clean 0.1 M $HClO_4$) agree well with previous work[39–42] and are shown in each figure below for reference. When scanning anodically (low to high potential), increases in mass are observed in the HUPD region (0.025 V–0.4 V), as well as in the Pt oxide formation region (>0.7 V), with a slight mass change in the double layer region. The mass increase observed in the low potential region is attributed to the net mass gain from hydrogen desorption and subsequent water and perchlorate ion adsorption. In the double-layer region, Jerkiewicz et al. suggested that the co-adsorbed anions (0.5 M $H_2SO_4$ in their experiments) slightly affect the mass change but has no impact on growth, since the anions desorb at the onset of surface oxide formation.[39] At the higher potential region, the almost linear mass gain observed with increasing potential is due to the formation of PtO oxide on the Pt surface, followed by an interfacial place exchange between $O_{chem}$ adatoms and the top-most Pt surface atoms, resulting in the formation of a quasi-3D surface lattice comprising $Pt^{2+}$ cations and $O^{2-}$ anions (i.e., the mechanism as described by Jerkiewicz et al.).[39,42–44] When scanning cathodically (i.e., reverse scan), the mass decreases as Pt oxide is reduced to Pt (ca. 1.2 V−0.7 V) and then decreases at a different rate (ca. < 0.4 V) as water and perchlorate ion desorb from and hydrogen adsorbs onto the Pt surface.

The voltammetry and EQCM responses in Figure 2, for a polycrystalline Pt electrode in the presence of 0.1 mM SA1 show no model compound adsorption. Both CV and EQCM curves in Figure 2 show close overlap of the baseline and model compound containing scans, indicating that the sulfonate compound SA1 is non-adsorbing. (It is assumed that the sulfonic acid end of SA1 is dissociated into the sulfonate form.) The absence of SA1's adsorption on polycrystalline Pt agrees with previous studies investigating triflic acid ($CF_3SO_3H$)[46,47] and PFSA ionomer.[45] There, the authors reported a weak interaction, i.e. non-specific adsorption, between the sulfonate anion and Pt surface. However, other CV, LSV, and surface enhanced Raman spectroscopy studies have reported that chemisorption of the sulfonate anion does occur when applying a Nafion ionomer film to a polycrystalline Pt surface.[48–50] It was suggested that film crystallization, from the ionomer film application method, may have enhanced the interaction between sulfonate groups and the Pt substrate.[45] Low concentrations and different structural nature (ionomer fragments in solution as opposed to an applied film) of the compound used in this study may also contribute to differences in the observations.

Results for the adsorption of 0.1 mM TFA are shown in Figure 3. Increases in both current and mass observed at ∼0.3 V in the CV and EQCM scans indicate interaction (adsorption) of the TFA anion with the Pt surface. Adsorption in this case most likely proceeds through each oxygen of the carboxylate anion of TFA, forming a bridged structure to the Pt surface. Such a bonding mechanism has been confirmed by previous researchers investigating adsorption of carboxylic acids on Pt surfaces.[40,41] For this reason, surface coverages were calculated assuming one model compound molecule i.e. carboxylate anion, per every two Pt sites.

Symmetry of the adsorption pattern at potentials lower than 0.3 V in both the CV scan and mass response suggests that the adsorption of TFA is a reversible process.[51] An increase in mass between 0.3 V to 0.7 V, followed by a small decrease in mass, suggests that TFA adsorption began immediately after leaving the HUPD region, and continued until oxide formation initiated. Interestingly, the CV shows no change resulting from TFA adsorption in the double layer region. This may be due to the interaction of the partially positive charged Pt surface (at a potential above the point of zero charge) with the negatively charged oxygen end of both the water molecule and the TFA carboxylate anion. This interaction takes place without any charge transfer, hence no change in the CV in the double layer region. However, the interactions are sufficiently strong to bring about a mass change.[39] Generation of oxides effectively displaced all adsorbed TFA from the surface, as indicated by the small mass decrease at the onset of oxide formation and then the overlap of the EQCM and CV signals at higher oxide formation potentials (>0.9 V). The reverse (cathodic) scan suggests that upon surface oxide reduction i.e. oxide removal, TFA effectively re-adsorbed onto the electrode surface until being removed again (in this case by adsorbing hydrogen) upon re-entering the HUPD region. Surface coverage of TFA was determined to be 36% and 2% at the peak coverage point (∼0.7 V) and 0.9 V, respectively. In summary, TFA physisorbs onto Pt surface and can be displaced by Pt oxides and hydrogen atoms. The observed minimal impact of the TFA anion on the PtO formation agrees with Furuya et al.'s study.[36]

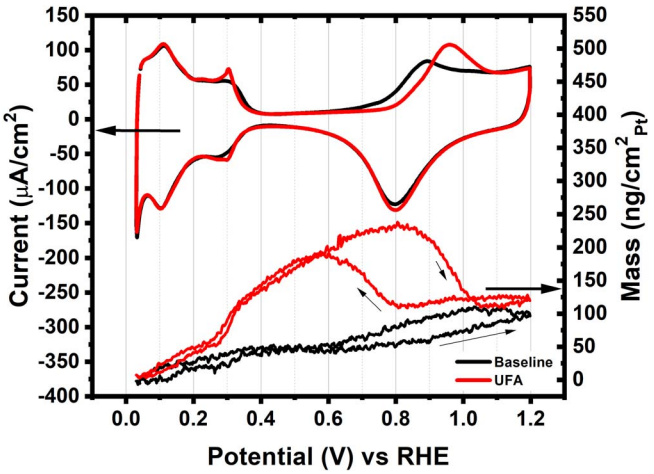


**Figure 4.** Voltammetric and EQCM response for UFA adsorption on polycrystalline Pt. Black: 0.1M $HClO_4$ baseline CV and EQCM, red: SA1 (0.1 mM in 0.1M $HClO_4$) CV and EQCM. Thin arrows show direction of EQCM scan.

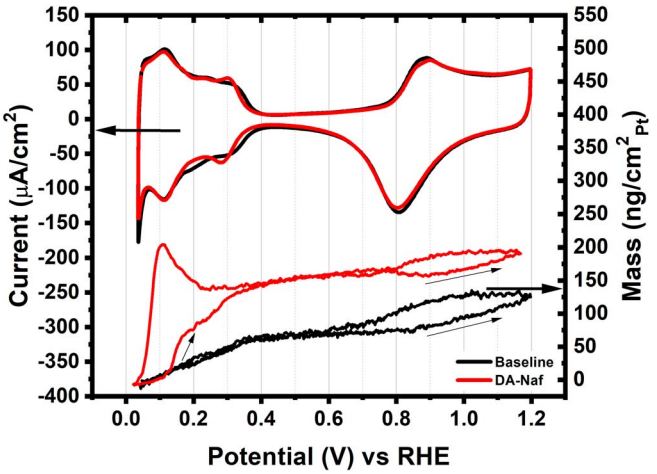


**Figure 5.** Voltammetric and EQCM response for DA-Naf adsorption on polycrystalline Pt. Black: 0.1M $HClO_4$ baseline CV and EQCM, red: SA1 (0.1 mM in 0.1M $HClO_4$) CV and EQCM. Thin arrows show direction of EQCM scan.

CV and EQCM responses for 0.1 mM UFA, shown in Figure 4, are similar but much more pronounced than those for TFA. Peaks observed in the CV scan indicate initial adsorption was occurring at a similar potential (0.3 V), although positive mass changes suggest that adsorption may be proceeding at lower potentials. A positive potential shift in oxide formation indicates that adsorption of UFA hindered Pt surface oxide generation. Shown in the anodic scan, maximum coverage occurred immediately before oxide formation initiated (∼0.8 V). A sharp decrease in mass measured as higher potentials were approached indicates displacement of the UFA compound from the electrode surface by lighter weight, oxide species. Differences in mass signals (UFA and baseline) at 1.2 V indicate UFA was present at the surface well into the oxide formation region. Hysteresis observed in the maximum adsorbed mass signals for the forward and reverse scans may represent differences in the amount of time available for adsorption to take place and/or different Pt surface state i.e. moving from a hydrogen or oxide covered surface to a free surface. Similar to TFA, mass begins to decrease as lower potentials are approached, lending further evidence to an anion adsorption process. UFA surface coverage was calculated to be 64% at highest coverage (∼0.8 V) and 50% at 0.9 V. (Surface coverage of TFA was determined to be 36% and 2% at the highest coverage point (∼0.7 V) and 0.9 V respectively). Increases in surface coverage for UFA compared with TFA is postulated to be related to the increased chain length of UFA, which allows for greater cohesive forces within the adsorbed organic layer, leading to higher molecular ordering of adsorbed species.[23]

EQCM results for diacid model compounds, DA-Naf and DA-3M, are shown in Figures 5 and 6, respectively. Both compounds showed similar adsorption behavior, with DA-3M exhibiting higher surface coverage than DA-Naf. In contrast to both TFA and UFA adsorption, both diacids exhibited consistently high surface coverages at all potentials above ∼0.3 V, even in the oxide region.

Interestingly, although it was reported in a recent study[23] that the impact on ORR kinetic current loss (measured at 0.9 V) was greater for DA-Naf and DA-3M compared with UFA, the surface coverages calculated here for both DA-Naf and DA-3M at 0.9 V were similar or less than UFA (Table I). Thus, it was determined that the terminal sulfonic acid group for both DA-Naf and DA-3M must be playing a role during molecular adsorption to the electrode surface while further hindering oxygen reduction from occurring. Two scenarios were postulated on the mechanism of the sulfonate group: either the sulfonate anion is contributing to a secondary adsorption (after initial adsorption through the carboxylate anion), leading to a greater number of Pt sites covered per molecule adsorbed; or, after initial carboxylate adsorption, sulfonate anions create a stable network through hydrogen bonding or other intermolecular forces, leading to greater steric hindrance and barrier for molecular oxygen to reach the surface.[23]

When comparing surface coverages calculated for the forward and reverse scan at 0.9 V, a significant difference is observed for UFA (45% decrease) compared with the diacids (5% and 14% decrease for DA-Naf and DA-3M, respectively. Greater surface coverage for the diacids during the reverse scan lends further evidence to their greater affinity for the oxide covered electrode surface than that of the mono-carboxylates.

Table I summarizes the results of all model compounds studied by EQCM here, and compares surface coverages at 0.1 mM with ORR kinetic current losses measured at the same concentration in a previous study.[23]

Surface coverages reported in Table I correlate well with the previously reported losses in ORR kinetic current at 0.1 mM concentrations.[23] The only data that appears anomalous would be that for UFA, which exhibited a surface coverage of 50% but affected ORR kinetic current by only 17%. Since ORR activities were reported at a slower scan rate (20 mV/s), more time was spent in the oxide formation potential region, (and hence greater surface oxide

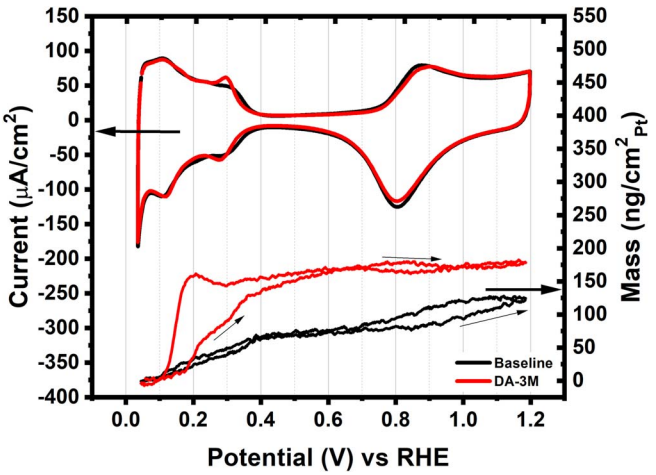


**Figure 6.** Voltammetric and EQCM response for DA-3M adsorption on polycrystalline Pt. Black: 0.1M $HClO_4$ baseline CV and EQCM, red: SA1 (0.1 mM in 0.1M $HClO_4$) CV and EQCM. Thin arrows show direction of EQCM scan.

**Table I. Summary of surface coverages and ORR kinetic current losses[22] measured for PEM degradation model compounds at 0.1 mM.**

| Compound | Structure | ORR kinetic current loss 0.9 V[22] | Surface coverage (θ) at 0.9 V (forward scan) | Surface coverage (θ) at 0.9 V (reverse scan) |
|---|---|---|---|---|
| SA1 | $CF_3—CF_2—CF_2—CF_2—SO_3H$ | < 5% | < 0.01 | < 0.01 |
| TFA | $HO—C(=O)—CF_3$ | < 5% | 0.05 ± 0.02 | < 0.01 |
| UFA | $HO—C(=O)—CF_2—CF_2—CF_2—CF_2—CF_3$ | 17% ± 1 | 0.50 ± 0.06 | 0.05 ± 0.04 |
| DA-Naf | $HO—C(=O)—CF(CF_3)—O—CF_2—CF_2—SO_3H$ | 44% ± 11 | 0.25 ± 0.02 | 0.19 ± 0.03 |
| DA-3M | $HO—C(=O)—CF_2—CF_2—CF_2—SO_3H$ | 47% ± 5 | 0.43 ± 0.05 | 0.29 ± 0.06 |

coverage),[52] than during the EQCM measurements taken at 50 mV/s. The extra time may have allowed greater amounts of UFA compound to be removed from the electrode surface before activity was measured at 0.9 V, thus lowering the effective surface coverage. This discrepancy may also suggest that oxygen reduction can still proceed even at Pt sites occupied by adsorbed carboxylate, suggesting the presence of a dynamic electrode/solution interface with reversible adsorption processes occurring simultaneously.

An alternative mechanism explaining the discrepancy between surface coverage and ORR kinetic current loss involves the known impact that a Pt oxide surface has on ORR kinetics. Previous reports have shown that Pt oxide decreases the kinetics of the ORR by changing the theoretical transfer coefficient from "0.5" to "1".[53] The hindering of surface oxide formation, due to UFA adsorption, results in a Pt surface with less oxide, which is more conducive for oxygen reduction. The surface coverages calculated for DA-Naf and DA-3M were assumed for a Pt-metal surface; however, continued mass changes into the oxide formation potential regime indicate that DA-Naf and DA-3M are adsorbing onto the Pt-oxide surface, likely through favorable interactions with the sulfonate group. Hence, lower oxide coverage in the case of UFA compared with DA-Naf and DA-3M would lend to improved ORR kinetics and a lower impact on kinetic current loss, which is what was observed.

High degrees of variance in surface coverages calculated during forward and reverse scans among UFA, DA-Naf, and DA-3M suggest that surface oxide coverage impacts adsorption of these compounds quite differently. Since an electrode surface fully covered in Pt oxide species is initially assumed during the reverse (cathodic) scan, it is clear based on reverse scan coverages that both diacid compounds have a greater affinity for the oxide surface than does UFA. When compared to forward (anodic) scan coverages, where surface oxides are not as developed, reverse scan measurements for DA-Naf and DA-3M show 21% and 46% decreases in coverage, whereas UFA shows a 90% decrease. Since the diacid compounds cannot be chemisorbed directly to the Pt surface while oxides are present, their significant influence on ORR kinetics must be related to a physisorbed affinity or direct bonding to the Pt-oxide layer. A longer, sterically hindered, more tortuous path for $O_2$ molecules to reach the underlying electrode surface is likely responsible for observed losses in ORR activity.

Higher surface coverage reported for DA-3M compared with DA-Naf may be due to a more favorable multilayer adsorption process taking place. Due to the presence of a fluoromethyl side chain in DA-Naf, the molecule is more sterically obstructive than that of DA-3M. The DA-3M molecular geometry therefore may be more conducive to intermolecular attraction among model compound chains which, in turn, could lead to a greater frequency response measured by the EQCM even though the amount of compound directly adsorbed to the surface may be similar between the diacids. This may also help explain the discrepancy between ORR kinetic current loss and θ for DA-Naf in Table I. In addition, if indeed the sulfonate group was also adsorbed to the surface, the surface coverage (calculated based on a 2:1 ratio of Pt sites to model compound) would be increased further due to more Pt sites being covered.

To obtain a more complete understanding of adsorption processes occurring for DA-Naf and DA-3M, measurements of surface coverages were also conducted at higher concentrations of 0.5 mM and 1 mM. Figures 7 and 8 show EQCM and CV responses for DA-Naf and DA-3M, respectively. Mass changes associated with both DA-Naf and DA-3M showed steadily rising values as concentrations increased. EQCM scan profiles were similar at all concentrations, however, overlap between the forward and reverse scans was not observed at concentrations above 0.1 mM.

When attempting to calculate surface coverage at concentrations higher than 0.1 mM, greater than 100% coverage was obtained for both compounds suggesting that more than one monolayer may have been present. Table II summarizes the surface coverages calculated for DA-Naf and DA-3M at 0.9 V for all concentrations studied.

Interactions among adsorbed species and those still in solution are feasible given their diacid, i.e dianionic nature and preferable hydrogen bonding conditions (due to the strong acid electrolyte environment). The surfactant nature of the model compounds themselves may also aid in intermolecular interactions due to the aggregation of hydrophobic segments of individual fluorocarbon chains and hydrophillic carboxylate and sulfonate functional groups.

While analyzing surface coverages at 0.9 V adds depth to the understanding of the relation between ORR activity losses and model compound concentrations, similar changes in mass observed for the adsorbing model compounds at lower potentials indicate that ORR

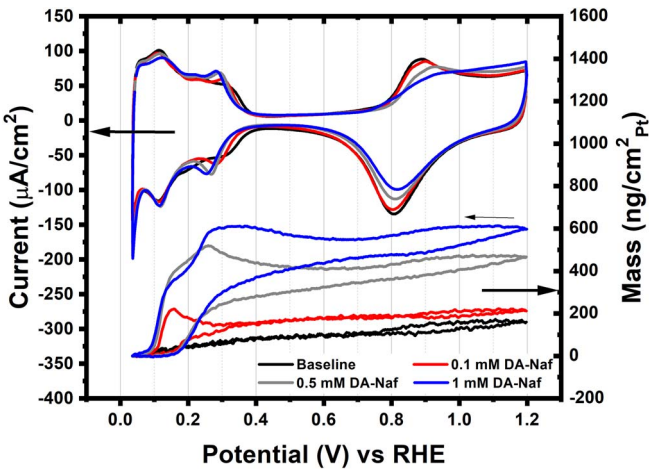


**Figure 7.** Voltammetric and EQCM response for polycrystalline Pt. Black: 0.1 M $HClO_4$ baseline, red: 0.1 mM DA-Naf in 0.1 M $HClO_4$, gray: 0.5 mM DA-Naf in 0.1 M $HClO_4$, blue: 1 mM DA-Naf in 0.1 M $HClO_4$. Thin arrows show direction of EQCM scan.

**Table II. Summary of calculated surface coverages at 0.9 V for DA-Naf and DA-3M at different concentrations.**

| Model Compound Concentration | Surface coverage (θ) of DA-Naf measured at 0.9 V | Surface coverage (θ) of DA-3M measured at 0.9 V |
|---|---|---|
| 0.1 mM | 0.24 ± 0.02 | 0.44 ± 0.05 |
| 0.5 mM | 0.89 ± 0.03 | 1.13 ± 0.30 |
| 1 mM | 1.22 ± 0.03 | 1.44 ± 0.15 |

performance may be affected at all relevant fuel cell operating conditions; a conclusion in agreement with an in-situ fuel cell study involving the injection of PEM degradation compounds.[27] Performance impact would seem especially true for the diacid compounds DA-Naf and DA-3M, which both showed consistent surface coverages at all potentials greater than ~0.2 V.

## Conclusions

Surface coverages of several model species representing PEM chemical degradation compounds were investigated using EQCM. All carboxylic acid containing model compounds demonstrated mass changes due to adsorption, while the model compound containing a sole sulfonic acid functional group showed no adsorption characteristics. This suggests that perfluoacid ionomers with a carboxylic acid group have a more negative impact on the PEM fuel cell durability than ionomers with sulfonic acid functional groups only. Although both perfluorocarboxylic acids TFA and UFA were effectively removed from the surface as electrode potentials moved into the oxide formation region, perfluorodiacids DA-Naf and DA-3M maintained surface coverage at higher potentials. The implication is that mitigation strategies such as potential control may be able to reverse the poisoning effect of carboxylic acid containing ionomers on the catalyst. Furthermore, the poisoning mechanism of an ionomer with two different acid groups is different from an ionomer with a single acid group. In conclusion, one needs to consider the length of the ionomer side chains, as well as the number and type of terminal functional groups when designing new ionomers for more durable fuel cells or ones that operates in harsher environments (i.e., drier and at higher temperature operation).[29,54]

Attempts to measure adsorption at higher concentrations for DA-Naf and DA-3M resulted in coverages of over 100%, suggesting adsorption greater than one monolayer. Although EQCM provides both qualitative and quantitative information in regards to anion adsorption, specific details about bonding mechanisms may only be attained through spectroscopic methods such as SEIRAS. Information gleaned from this study, along with others investigating fundamental adsorption processes of contaminating compounds, can contribute toward a better understanding of the contamination mechanism of membrane degradation products with different functional groups, and ultimately help design better, more durable membranes that do not degrade to products that will poison the fuel cell and shorten its life.

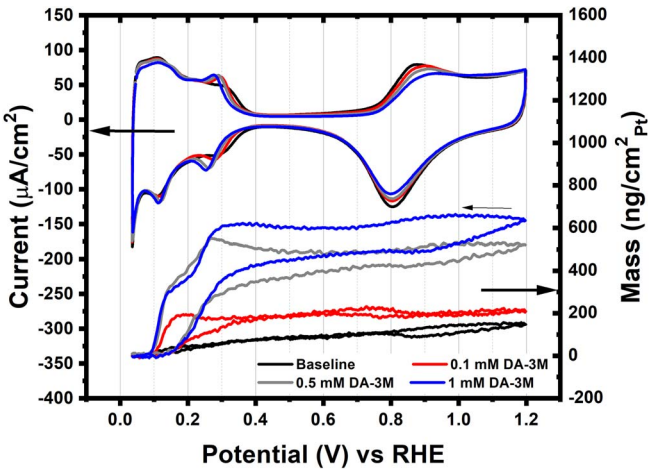


**Figure 8.** Voltammetric and EQCM response for polycrystalline Pt. Black: 0.1 M $HClO_4$ baseline, red: 0.1 mM DA-3M in 0.1 M $HClO_4$, gray: 0.5 mM DA-3M in 0.1 M $HClO_4$, blue: 1 mM DA-3M in 0.1 M $HClO_4$. Thin arrows show direction of EQCM scan.

## Acknowledgments

This work was fully supported by the U. S. Department of Energy (USDOE), Office of Energy Efficiency and Renewable Energy (EERE), Fuel Cell Technologies Office (FCTO), under contract no. DE-AC AC36-08GO28308 with Alliance for Sustainable Energy, LLC, the Manager and Operator of the National Renewable Energy Laboratory. The authors thank collaborators at 3M for providing model compounds DA-Naf and DA-3M, and also Metrohm Inc. for providing EQCM electrodes used in this study.

## ORCID

Huyen N. Dinh https://orcid.org/0000-0002-0284-8203

## References

1. Department of Energy, *Multi-Year Research, Development, and Demonstration Plan: Fuel Cells Section*, **3.4**, 1, (2016).
2. J. St-Pierre, in *Polymer Electrolyte Fuel Cell Durability*, F. Büchi, M. Inaba, and T. Schmidt, eds., p. 289, Springer New York, (2009).
3. Y. Garsany, O. A. Baturina, and K. E. Swider-Lyons, *Journal of the Electrochemical Society*, **154**(7), B670 (2007).
4. R. Halseid, T. Bystron, and R. Tunold, *Electrochimica Acta*, **51**(13), 2737 (2006).
5. J. St-Pierre, *Journal of Power Sources*, **196**(15), 6274 (2011).
6. J. St-Pierre, *International Journal of Hydrogen Energy*, **36**(9), 5527 (2011).
7. M. Nilsson, X. Karatzas, B. Lindstrom, and L. J. Pettersson, *Chemical Engineering Journal*, **142**(3), 309 (2008).
8. K. Kortsdottir, R. W. Lindstrom, T. Akermark, and G. Lindbergh, *Electrochimica Acta*, **55**(26), 7643 (2010).
9. J. J. Baschuk and X. G. Li, *Int. J. Energy Res.*, **25**(8), 695 (2001).
10. J. J. Zhang, H. J. Wang, D. P. Wilkinson, D. T. Song, J. Shen, and Z. S. Liu, *Journal of Power Sources*, **147**(1–2), 58 (2005).
11. X. Zhang, H. M. Galindo, H. F. Garces, P. Baker, X. Wang, U. Pasaogullari, S. L. Suib, and T. Molter, *Journal of the Electrochemical Society*, **157**(3), B409 (2010).
12. X. Zhang, U. Pasaogullari, and T. Molter, *International Journal of Hydrogen Energy*, **34**(22), 9188 (2009).
13. C. Macomber, H. Wang, K. O'Neill, S. Coombs, G. Bender, B. Pivovar, and H. N. Dinh, *ECS Transactions*, **33**(1), 1637 (2010).
14. C. S. Macomber, J. Christ, H. Wang, B. S. Pivovar, and H. N. Dinh, *ECS Transactions*, **50**(2), 603 (2013).
15. M. S. Opu, M. Ohashi, H.-S. Cho, C. S. Macomber, H. N. Dinh, and J. W. Van Zee, *ECS Transactions*, **50**(2), 619 (2013).
16. H. Wang, S. Coombs, C. Macomber, K. O'Neill, G. Bender, B. Pivovar, and H. N. Dinh, *ECS Transactions*, **33**(1), 1617 (2010).
17. H. Wang, C. Macomber, J. Christ, G. Bender, B. Pivovar, and H. N. Dinh, *Electrocatalysis*, **5**(1), 62 (2014).
18. H. Wang, C. S. Macomber, and H. N. Dinh, *ECS Transactions*, **50**(2), 659 (2013).
19. C. Zhou, M. A. Guerra, Z. M. Qiu, T. A. Zawodzinski, and D. A. Schiraldi, *Macromolecules*, **40**(24), 8695 (2007).
20. L. Ghassemzadeh, K.-D. Kreuer, J. Maier, and K. Müller, *The Journal of Physical Chemistry C*, **114**(34), 14635 (2010).
21. J. Healy, C. Hayden, T. Xie, K. Olson, R. Waldo, A. Brundage, H. Gasteiger, and J. Abbott, *Fuel Cells*, **5**(2), 302 (2005).
22. M. Emery, M. Frey, M. Guerra, G. Haugen, K. Hintzer, K. H. Lochhaas, P. Pham, D. Pierpont, M. Schaberg, A. Thaler, M. Yandrasits, and S. Hamrock, *ECS Transactions*, **11**(1), 3 (2007).
23. J. M. Christ, K. C. Neyerlin, H. Wang, R. M. Richards, and H. N. Dinh, *Journal of The Electrochemical Society*, **161**(14), F1481 (2014).

24. J. M. Christ, K. C. Neyerlin, R. M. Richards, and H. N. Dinh, *Journal of The Electrochemical Society*, **161**(14), F1360 (2014).
25. M. Chen, C. Du, J. Zhang, P. Wang, and T. Zhu, *Journal of Power Sources*, **196**(2), 620 (2011).
26. N. M. Markovic, H. A. Gasteiger, B. N. Grgur, and P. N. Ross, *Journal of Electroanalytical Chemistry*, **467**(1–2), 157 (1999).
27. A. Kabasawa, H. Uchida, and M. Watanabe, *Electrochemical and Solid State Letters*, **11**(10), B190 (2008).
28. R. Borup, J. Meyers, B. Pivovar, Y. S. Kim, R. Mukundan, N. Garland, D. Myers, M. Wilson, F. Garzon, D. Wood, P. Zelenay, K. More, K. Stroh, T. Zawodzinski, J. Boncella, J. E. McGrath, M. Inaba, K. Miyatake, M. Hori, K. Ota, Z. Ogumi, S. Miyata, A. Nishikata, Z. Siroma, Y. Uchimoto, K. Yasuda, K.-I. Kimijima, and N. Iwashita, *Chemical Reviews*, **107**(10), 3904 (2007).
29. M. Yandrasits, M. Lindell, D. Peppin, A. Komlev, S. Hamrock, G. Haugen, E. Fort, and K. Kalstabakken, *Journal of The Electrochemical Society*, **165**(6) F3261 (2018).
30. S. Gilman, *Electrochimica Acta*, **65**, 141 (2012).
31. J. M. Orts, R. Gomez, J. M. Feliu, A. Aldaz, and J. Clavilier, *Electrochimica Acta*, **39**(11–12), 1519 (1994).
32. M. Osawa, "Surface-Enhanced Infrared Absorption" Book Chapter. S. Kawata (Ed.): Near-Field Optics and Surface Plasmon Polaritons, *Topics Appl. Phys.*, **81**, 163 (2001).
33. G. Sauerbrey, *J. Phys.*, **155**, 206 (1959).
34. J. Kim and G. Jerkiewicz, *Analytical Chemistry*, **89**(14),7462 (2017).
35. J. Kim, P. Urchaga, S. Baranton, C. Coutanceau, and G. Jerkiewicz, *Physical Chemistry Chemical Physics*, **19**(33), 21955 (2017).
36. Y. Furuya, T. Mashio, A. Ohma, M. Tian, F. Kaveh, D. Beauchemin, and G. Jerkiewicz, *ACS Catalysis*, **5**(4), 2605 (2015).
37. M. C. Santos, D. W. Miwa, and S. A. S. Machado, *Electrochemistry Communications*, **2**, 692 (2000).
38. T. W. Schneider and D. A. Buttry, *J. Am. Chem. Soc.*, **115**, 12391 (1993).
39. G. Jerkiewicz, G. Vatankhah, J. Lessard, M. P. Soriaga, and Y. S. Park, *Electrochimica Acta*, **49**(9–10), 1451 (2004).
40. E. Pastor, A. Rodes, and T. Iwasita, *Journal of Electroanalytical Chemistry*, **404**(1), 61 (1996).
41. A. Rodes, E. Pastor, and T. Iwasita, *Journal of Electroanalytical Chemistry*, **376**(1–2), 109 (1994).
42. G. Jerkiewicz, G. Vatankhah, S. I. Tanaka, and J. Lessard, *Langmuir*, **27**(7), 4220 (2011).
43. M. C. Santos, D. W. Miwa, and S. A. S. Machado, *Electrochemistry Communications*, **2**(10), 692 (2000).
44. K. Shimazu and H. Kita, *Journal of Electroanalytical Chemistry*, **341**(1), 361 (1992).
45. T. Masuda, F. Sonsudin, P. R. Singh, H. Naohara, and K. Uosaki, *J. Phys. Chem. C*, **117**(30), 15704 (2013).
46. A. Berna, J. M. Feliu, L. Gancs, and S. Mukerjee, *Electrochemistry Communications*, **10**(11), 1695 (2008).
47. M. Teliska, V. S. Murthi, S. Mukerjee, and D. E. Ramaker, *J. Phys. Chem. C*, **111**(26), 9267 (2007).
48. R. Subbaraman, D. Strmcnik, V. Stamenkovic, and N. M. Markovic, *J. Phys. Chem. C*, **114**(18), (2010).
49. R. Subbaraman, D. Strmcnik, A. P. Paulikas, V. R. Stamenkovic, and N. M. Markovic, *Chemphyschem*, **11**(13), (2010).
50. J. Zeng, D.-I. Jean, C. Ji, and S. Zou, *Langmuir*, **28**(1), (2012).
51. A. J. Bard and L. R. Faulkner, *Electrochemical Methods: Fundamental and Applications*, 2nd Edition, (2001).
52. B. Conway, B. Barnett, H. Angerstein-Kozlowska, and B. Tilak, *The Journal of chemical physics*, **93**(11), 8361 (1990).
53. N. P. Subramanian, T. A. Greszler, J. Zhang, W. Gu, and R. Makharia, *Journal of The Electrochemical Society*, **159**(5) B531 (2012).
54. M. Yandrasits, M. Lindell, M. Schaberg, and M. Kurkowski, *The Electrochemical Society Interface*, **26**(1), 49 (2017).